Research Square

Preprints are preliminary reports that have not undergone peer review.
They should not be considered conclusive, used to inform clinical practice,
or referenced by the media as validated information.

In vitro hydrogel-cell model for pharmacokinetic analysis

Moira Lorenzo Lopez
University of Liverpool
Victoria Kearns
Vkearns@liverpool.ac.uk
University of Liverpool
Eann Patterson
University of Liverpool
Jude Curran
University of Liverpool

Research Article

Keywords: hydrogel-cell, interface, nanoparticles, label-free, vitreous humour, pharmacokinetics

Posted Date: November 5th, 2026

DOI: https://doi.org/10.21203/rs.3.rs-11431965/v1

License: This work is licensed under a Creative Commons Attribution 4.0 International License.
Read Full License

Additional Declarations: Competing interest reported. VK is a member of the editorial board of the journal In vitro models otherwise the authors declare no competing interests.

In vitro hydrogel-cell model for pharmacokinetic analysis

Moira Lorenzo Lopez[1,2] (Orcid:0000-0002-8279-7118), Victoria R. Kearns[2*] (Orcid:0000-0003-1426-604), Eann A. Patterson[1] (Orcid:0000-0003-4397-2160), Judith M. Curran[1] (Orcid:0000-0003-1551-2917).

[1]School of Engineering, University of Liverpool, Liverpool L69 3BX, UK.

[2]Department of Eye and Vision Science, University of Liverpool, Liverpool L7 8TX, UK.

*Corresponding author: Vkearns@liverpool.ac.uk

Abstract

Purpose:

Understanding nanoparticle interactions and transport across hydrogel matrices and their associated interface with cellular layers is essential for designing effective drug delivery systems, tissue engineering scaffolds, and biomaterial platforms. Therefore, robust in vitro models that simulate complex extracellular matrices and that support quantitative transport analysis are crucial as preclinical screening tools.

Methods:

This study presents the development of a versatile, multicomponent in vitro hydrogel-cell model designed to evaluate nanoparticle transport dynamics and boundary layer interactions, demonstrated here using an optimised synthetic vitreous humour analogue and an adherent retinal cell (ARPE-19) layer as a representative model. This is achieved by exploiting the capabilities of an emerging label-free nanoparticle tracking platform, which can dynamically characterise the effects of matrix complexity, protein interactions, and cellular presence on gold nanoparticle transport in real time.

Results:

The model effectively characterised how increasing system complexity influenced nanoparticle diffusion. In serum-rich media, nanoparticles incubated for 24 h showed significantly higher diffusion rates when compared to serum-free media, suggesting the presence of nanoparticle-protein interactions that prevented particle-particle aggregation. The introduction of an ARPE-19 cell layer further increased biological complexity reflected by greater variability in nanoparticle diffusion. Finally, the addition of the hydrogel matrix resulted in a bimodal diffusion distribution, successfully resolving the distinct aqueous and gel phase microenvironments within the model.

Conclusion:

This experimental model provides a quantitative framework for evaluating how nanoentity properties govern carrier-protein interactions, matrix diffusion, and target cell delivery. Ultimately, these insights will inform nanocarrier design to control transport across complex biomaterials and biological interfaces.

Key words: hydrogel-cell, interface, nanoparticles, label-free, vitreous humour, pharmacokinetics.

Introduction

The boundary where hydrogels meet cellular layers plays a critical role in controlling how drugs and nanoparticles move, interact with proteins, and reach their target cells. This dynamic environment is central to many biomedical applications, including disease modelling, soft tissue regeneration, drug delivery, and cell-biomaterial scaffolds [1–3]. In these systems, dense extracellular matrix networks actively dictate nanocarrier permeation, surface adsorption, and localised cellular uptake. These models provide valuable platforms for studying cell interactions, disease modelling, and therapeutic developments. If designed and characterised appropriately, in vitro systems offer controlled environments with high reproducibility, providing more cost-effective and ethical solutions when compared to in vivo or ex vivo models [4].

Traditional in vitro models used for drug development and diseases modelling have been based on a monolayer of cells, grown usually in a petri dish or flask. Despite their simplicity and reproducibility, these models are now being replaced with more complex 3D structures, due to their limited ability to replicate the complex physical and biochemical barriers in the biological environment. Recent research efforts have focused on replicating the complexity of the stratified nature of different tissues, such as skin or the retina, with 3D in vitro models [5,6]. This has resulted in the production of more complex and accurate physiological models to study tissue function and disease [7]. These advanced in vitro models enable the investigation of physiology and physiopathology at the biochemical level, in a more biologically relevant environment, where interactions between different cell types and microfluidics are replicated [6]. In addition, recent efforts have focused on predicting patient-specific drug responses, further highlighting the potential of these systems in translational research [8].

However, when it comes to drug development and drug design these research models study the drug's action once the drug is already in the target cell layer, overlooking the transport barriers encountered en route. A clinically critical example of this challenge is found in the treatment of retinal diseases. Retinal drug delivery can occur through four principal routes of administration: intravitreal, subretinal, suprachoroidal and systemic [9,10]. Intravitreal administration is the most common method currently used in clinic, where a single hospital in London, UK has forecasted 83,000 intravitreal injections for 2029 [11].This method is used for the treatment of diabetic retinopathy (DR) and age-related macular degeneration (AMD), which are two of the most common retinal affecting pathologies, [12]. Following intravitreal injection, the drug, despite being delivered close to the retina, has first to efficiently migrate from the injection site to the targeted tissue, through the vitreous humour, a factor that is not incorporated into many in vitro models.

Relying on models that assume that the drug concentration reaching the cellular interface is the same as the administrated drug concentration can lead to an overinterpretation of the efficacy and misinterpretation of the cellular response [13]. Therefore, for the design of novel therapeutics and to assess a safe and effective posology, it is essential to evaluate the drug's pharmacokinetics accounting for the initial hydrogel-like matrix. The vitreous humour serves here as a model of biological barrier that the nanocarriers must overcome to reach the targeted tissue, the retina [14].

The vitreous humour is a complex viscoelastic gel that fills the space between the lens and the retina. It is made up of water (98%), a matrix of collagen stabilised with hyaluronic acid, glycosaminoglycans, proteins and ions. This matrix and the multiple components of the vitreous can restrict the drugs' transport in a physical or chemical manner, where properties such as drug/nanocarrier size and charge can define the fate of the therapeutic [15,16].

Previous in vitro research tested hydrogels based on agar and hyaluronic acid as vitreous humour substitutes [17,18]. These hydrogels, where agar aims to mimic the easy-degradable collagen mesh naturally occurring in the vitreous, were presented as a more stable solution when compared to the extraction of vitreous from cadaveric eyes. Our recent work demonstrated that the lowest tested concentrations of agar and hyaluronic acid (0.95 mg/mL and 0.7 mg/mL, respectively) most accurately recapitulate the mechanical and morphological properties of porcine vitreous humour [18,19].

Since much current retinal drug research is based on long-acting therapies that can increase the drug's half-life in the ocular chamber, nanoparticles are being considered a promising platform to encapsulate already existing drugs, to stabilise them in the vitreous humour, or to increase their bioavailability, thus reducing the total number of intravitreal injections needed in the overall treatment [20–22].

It is essential to account for the presence of proteins in the media in models evaluating nanoparticle-based drug delivery systems. Extensive research on nanoparticle–protein interactions has established that, upon exposure to biological fluids, nanoparticles rapidly and spontaneously adsorb proteins onto their surface, forming a dynamic coating known as the protein corona [23,24]. This corona can change the inherent properties of the nanoparticle, making it a new entity that may no longer reflect the characteristics of the native form [25]. This change in the properties of the surface of the nanoparticles can affect their transport and fate in biological environments [26–28]. Consequently, nanoparticle-protein interactions are a critical consideration in therapeutic design and pharmacokinetic analyses. Although the protein concentration in the vitreous humour is low (4.7±1.2 mg/mL) [15] when compared to other biological fluids such as blood (65-81 mg/mL) [29], their influence on nanoparticle transport should be accounted for when performing pharmacokinetic analysis.

The most used cell line for retinal in vitro models is the ARPE-19, a well-established human-derived retinal pigmented epithelial (RPE) cell line isolated from a 19-year-old donor [5,30]. First established and characterised in 1996 they have since become a standard model for retinal research due to their growth capacity and consistency, as they are an immortalise cell line with the same original donor [31]. Although ARPE-19 cells lack some native RPE properties and phenotypic characteristics and represents the RPE monolayer rather than the full neurosensory retina, they remain widely used in vitro due to their ease of cultivation and high experimental reproducibility, making them well-suited for model development [32].

Current techniques to assess nanoparticle transport across complex media, involve the use of lasers or the addition of fluorescent tags (such as nanoparticle tracking analysis- NTA, super-resolution microscopy- SRM, and confocal microscopy) [33,34]. However, for dynamic nanoparticle visualisation and tracking, these approaches are limited in their ability to provide accurate and highly reproducible quantitative data [35]. Laser-based methods can highly influence cell viability through phototoxicity, while the addition of fluorescent tags can alter the physicochemical properties of the nanoparticles, changing their interactions with proteins in solution and with the vitreous analogue, affecting the fate of the nanoparticles [36–38].

To address these limitations, we propose the use of an emerging platform originated from applying the natural phenomena of caustics in an optical inverted microscope. Based on light refraction, this technique has recently proven useful to investigate nanoparticle transport in a label-free and dynamic manner [19,39,40]. This platform enables the visualisation of nanoparticles, with minimal sample preparation, without the use of labels that can affect the nature of the nanoparticle interaction with the model, avoiding these steps the platform provides more reproducible and accurate values of diffusion [41].

This study aims to develop a versatile, multicomponent in vitro platform designed for the pharmacokinetic evaluation and optimisation of nanoparticle-based drug delivery systems across complex biological barriers. The proposed platform addresses a critical gap in the literature by enabling pharmacokinetic analysis that accounts for the vitreous humour and a subretinal cell layer. The model is presented as a user-friendly, reproducible, and cost-effective platform for investigating nanoparticle transport across a developed vitreous analogue toward an ARPE-19 cell layer using standard optical microscopy.

To establish the foundation of the model, the effects of nanoparticle-protein interaction and nanoparticle surface charge on the diffusion of the investigated nanoparticles (100 nm positively and negatively charged gold nanoparticles) were first evaluated in the absence of the cell layer.

Subsequently the same nanoparticles were used to examine how those parameters are affected by the incorporation of cells. Finally, nanoparticle distribution and interactions were assessed with the hydrogel matrix (the optimised vitreous analogue), validating the multicomponent model for in vitro analysis.

Materials and methods

Nanoparticles

100 nm (-32.7 mV) spherical citrate-capped gold nanoparticles (AuNPs) were purchased from BBI Solutions (Crumlin, UK), and 100 nm diameter (28.7 mV) branched polyethylenimine (BPEI) capped AuNPs were obtained from NanoComposix. These nanoparticle stock solutions (10^{-2} mg/mL) were diluted in ultra-pure deionized water to obtain the desired constant concentration of 10^{-7} particle/mL when added to each tested formulation.

Cell culture media

Dulbecco's Modified Eagle's Medium: nutrient mixture F12 (DMEM/F12) (11320-033 Gibco, UK), foetal bovine serum (FBS) (Gibco, UK), Penicillin-Streptomycin (10,000 U/mL) (Gibco, UK), Trypsin-EDTA (0.25%), phosphate buffered saline (PBS) (10X) (Gibco, UK).

ARPE-19 Cell line expansion

Human retinal pigmented epithelial cell line (ARPE-19, ATCC CRL-2302)) at passage 25 were cultured in Dulbecco's Modified Eagle's Medium: nutrient mixture F12 (DMEM/F12) (Gibco, UK), with 10% (v/v) foetal bovine serum (FBS), 100 U/mL penicillin, and 100 µg/ mL streptomycin under standard culture conditions (37˚C, 5% CO_2). When 80% confluent ARPE-19 cells were passaged. Cells were washed twice with 5 mL phosphate buffered saline (PBS) solution, trypsinised to detach them from the flask and centrifuged at 300 g for 5 min. Cells were resuspended in complete culture medium (DMEM F12+ 10% FBS + pen/strep) and seeded 1:3 in T75 flask.

Vitreous humour analogue synthesis

Asgar and hyaluronic acid hydrogels used as a vitreous substitute were synthesised using previously described methods [18]. To a 1X boiling phosphate buffer saline (PBS) solution the following were added: agar at a concentration of 0.95 mg/mL and hyaluronic acid (high molecular weight) at a concentration of 0.7 mg/mL. The solution was magnetically stirred (500-1000 rpm) at 100˚C for 1 hour, after which the agar hyaluronic acid hydrogel (AHA) was cooled down at room temperature overnight before being mixed with different ratios of the previously filtered (with a 0.22 µm PES sterile filter) DMEM/F12 + 10% FBS media.

Vitreous humour analogue cytotoxicity assay

To ensure that the microscope glass coverslips (22 mm^2) did not affect ARPE-19 cells viability and surface attachment, cells cultured on coverslips were compared to cells cultured in the well of a standard cell culture dish. At the same time the vitreous analogue was assess for cytotoxicity.

In a cell culture treated 6-well plate, coverslips were placed inside three of the wells while the other three were left empty. ARPE-19 cells were seeded at a density of 2.0×10^5 cells per well and incubated for 48h to allow the formation of a confluent monolayer. The media was then changed, and the cells were washed twice with PBS prior to incorporating the different ratios of DMEM/F12 + 10% FBS (full media): AHA. Three environments (test media) were tested both with and without coverslips, the first one full media alone, a second 50% (v/v) full media and 50% (v/v) AHA hydrogel, and the third the AHA hydrogel alone. These different media were left to incubate for 24 h. A qualitative assessment was performed through the comparison of images taken of the cells with an optical microscope, of the untreated (prior to adding the test media) and treated (after the 24 h incubation with the test media), to compare qualitatively the cytotoxicity effect of the vitreous humour analogue and the presence of microscope glass coverslips through the cell morphology.

A second qualitative assay was performed to assess the optimisation of the vitreous analogue through the combination of different ratios of full media and the AHA hydrogel. ARPE-19 cells were seeded onto 6-well plates (with microscope glass coverslips) following the same procedure as stated above. Six different conditions were tested, full media alone, 60% AHA hydrogel with 40% full media, 70% AHA hydrogel with 30% full media, 80% AHA hydrogel with 20% full media, 90% AHA hydrogel with 10% full media, and AHA hydrogel alone. The assessment was performed through the comparison of images taken of the cells in an optical microscope, of the untreated (prior to adding the test media) and treated (after the 24 h incubation with the test media), to qualitatively compare the cytotoxicity effect of the vitreous humour analogue through the cell morphology.

Resazurin assay

The same plates used for the second qualitative assay were used to perform a resazurin assay. 1 mL of a filtered (0.22 µm PES sterile filter) complete media with 11 µg/mL resazurin sodium salt (Sigma, #199303) was added per well after discarding previous media and washing twice with PBS. The plates were left to incubate at 37 ˚C, 5% CO_2 for 2h. After 2 h incubation the supernatant of each well was collected and added into a black 96-well plate (in triplicate) for fluorescent reading

at 570 nm, in a Synergy HT microplate reader (BioTek, USA). A blank of only the 10% resazurin solution in full media without cells served as background control.

Nanoparticle tracking

The diffusion coefficient of positively-charged 100 nm AuNP and negatively-charged 100 nm AuNP, with a final particle concentration of 10^{-7} particle/mL was evaluated at 37°C. An aliquot of 50 µL of the sample (test media containing AuNPs) was added into the cavity of a microscope slide (76x26 mm and 0.2 mm cavity depth), and sealed with a microscope glass coverslip of 22 mm x 22 mm. The samples were incubated on the microscope stage-top incubation system at 37°C for 10 minutes prior to being analysed under an Axio Observer.Z1 m (Carl Zeiss, DE) inverted optical microscope, to ensure a consistent temperature throughout the sample. Label-free nanoparticle tracking was achieved by increasing the coherence of the light, by closing the aperture of the condenser to its minimum (approximately 1 mm), adding a green interference filter (Olympus, JP, centred on 550 nm, 45 nm bandwidth), and setting the microscope for Köhler illumination by adjusting the condenser height to where the light throughput was maximised; following the methodology described by Patterson and Whelan [41,42]. Videos of individual nanoparticles trajectories were recorded using a x 40 objective and a monochromatic camera (Axiocam305, Carl Zeiss, DE) with a spatial resolution of 0.086 μm^2 for one pixel and a temporal resolution of 92 fps.

To determine the effect of nanoparticle-protein interactions on the diffusion of nanoparticles through cell culture media, two different media were tested for each charge of nanoparticles, DMEM/F12 (serum-free) and DMEM/F12 enriched with 10% FBS. Once the nanoparticles were added into each media the samples were vortexed (with a Vortex-Fisherbrand® mixer, UK) for 15 s and ultrasonicated (with a S-Series Heated Ultrasonic Bath Fisherbrand®, UK) for 1 minute. The incubation time of the nanoparticles was also assessed in both media at two different time points, 10 minutes and 24 h incubation at 37 ˚C, 5% CO_2, aligning with the cell culture conditions. After the 24 h incubation, the effect of sample sonication prior to analysis was also assessed, so the samples were first analysed without being sonicated and then they were analysed after 1 minute of sonication. A total of six nanoparticles, randomly selected from the field of view, were tracked for each set of conditions and this was performed in triplicate.

For the analysis of nanoparticle diffusion above the ARPE-19 cell monolayer, three different media were tested: DMEM/F12 (serum-free), DMEM/F12 enriched with 10% FBS, and the vitreous analogue (80% AHA hydrogel and 20% DMEM/F12 enriched with 10% FBS). Firstly, a confluent monolayer of ARPE-19 cells was obtained as described above, on a microscope glass coverslip

of 22 mm x 22 mm. Secondly, to test the influence of protein interactions and the proximity to the cell layer on the nanoparticle diffusion, nanoparticles (positively and negatively charged separately) were added to the protein-enriched and protein-free DMEM/F12 media, and tracked at 25 μm and 50 μm from the surface of the cell monolayer. A total of six nanoparticles, randomly selected from the field of view, were tracked for each set of conditions and this was performed in triplicate. Finally, to test the multicomponent model, nanoparticles (positively and negatively charged separately) were added to the vitreous analogue and 20 nanoparticles were randomly selected and tracked over time above the ARPE-19 cell monolayer at both distances (25 and 50 μm) and these were then compared to the nanoparticle diffusion on the vitreous analogue without the influence of the ARPE-19 cells.

Data analysis

The obtained videos of the nanoparticles motion were analysed using the ImageJ software plugin TrackMate [43]. This provided information on the x and y coordinates of the nanoparticle within the image plane for each successive frame. These coordinates mapped the path of the NPs over time, enabling the extraction of mean squared displacement (MSD) and hence to determine the nanoparticle's diffusion coefficient, as there is a linear relation between the mean squared displacement and the diffusion coefficient (D), for Brownian motion, for a specific time lag (Δt), in a dimension (d) (in this case 2D) [44,45]:

$$D = \frac{MSD}{2d\Delta t} \quad [1]$$

A correlation analysis between the area containing the path of a nanoparticle and the value of its diffusion coefficient was performed to better understand the nanoparticles' interaction and distribution through the vitreous analogue. For that the area of the smallest polygon enclosing all the nanoparticle positions (convex hull) in 100 frames, was calculated through a geometric algorithm (in MATLAB, R2025b)[46]. These values of the area were then correlated to the obtained experimental diffusion coefficient values, for each nanoparticle, following the same procedure as Lorenzo et al.[19]. Moreover, a frequency distribution analysis (OriginPro®, 2026) was performed to better visualise the nanoparticle's distribution through the vitreous analogue hydrogel.

Statistical analysis

Statistical analysis was performed through a linear mixed-effects model to account for the hierarchical structure and dependency of the data where the nanoparticles were nested into sample formulations were considered as the random effects, and the fixed effects were

considered to be the different tested factors (media, incubation time, charge, sonication and distance from the cell monolayer) that can modulate the nanoparticle diffusion. This was executed using the lmer() function in R's lme4 package, where assumptions of normality for residuals were checked using Q-Q plots. p values < 0.05 and < 0.001 were considered statistically significant and highly significant, respectively.

Results and discussion

Protein interaction effect on nanoparticle diffusion in cell culture media

Gold nanoparticles were selected due to their widespread use and characterisation in the literature, and a single size (100 nm) was investigated to reduce the number of variables [47,48].

With the aim of investigating the effect of nanoparticle-protein interaction and surface charge on nanoparticle transport when nanoparticles are used in biological environments, both positively surface charge 100 nm gold nanoparticles capped with BPEI, and negatively surface charge 100 nm citrate-capped gold nanoparticles were incubated separately for different times (10 min and 24 h) in serum-free cell culture media (DMEM/F12) and protein-rich cell culture media (DMEM/F12 +10% FBS). These particles were tracked avoiding the use of fluorescent labels, in an optical inverted microscope, to obtain more reliable experimental values of their diffusion coefficients [38,41].

As shown in Figure 1, nanoparticle diffusion values for both surface charges in protein-free media (DMEM/F12) following 24 h incubation experienced a 2-fold decrease (p< 0.0001) when compared with diffusion measured after 10 min in the same medium. More interestingly, NP diffusion at 24 h in protein-free media was also reduced relative to that observed in protein-rich media (DMEM/F12 + 10% FBS) for the same incubation time. However, at the same time the nanoparticles incubated in DMEM/F12 +10% FBS for 24 h showed 1.35 times increase (p=0.024) when compared to their diffusion obtained after 10 minutes of incubation.

These results align with previous studies on how nanoparticle-protein interactions affect the dynamics of nanoparticles [23,25,49]. This can be explained with the Vroman effect, a dynamic dual chemical effect that the presence of proteins in the media can have over nanoparticles depending on protein concentration and incubation time [50]. When the protein concentrations are low, the weak interactions can make the nanoparticles more prone to particle-particle aggregation after a long period of incubation (i.e. 24 h), due to the high ionic strength that reduces the electrostatic repulsion between the NPs that causes the formation of large aggregates, which diffuse slowly [51]. However, in the presence of a high protein concentration, such as used to

mimic biological environments, proteins present in high concentrations can be absorbed by the nanoparticles quickly (i.e. 10 min), and over time (i.e. 24 h) other proteins are believed to interact with the particles, strengthening their bonds with the surface of nanoparticles [52]. This creates a stable though dynamic protein interaction with nanoparticles' surface, which has the ability to stabilise the solution preventing particle-particle aggregation, due to the steric hindrance [53].

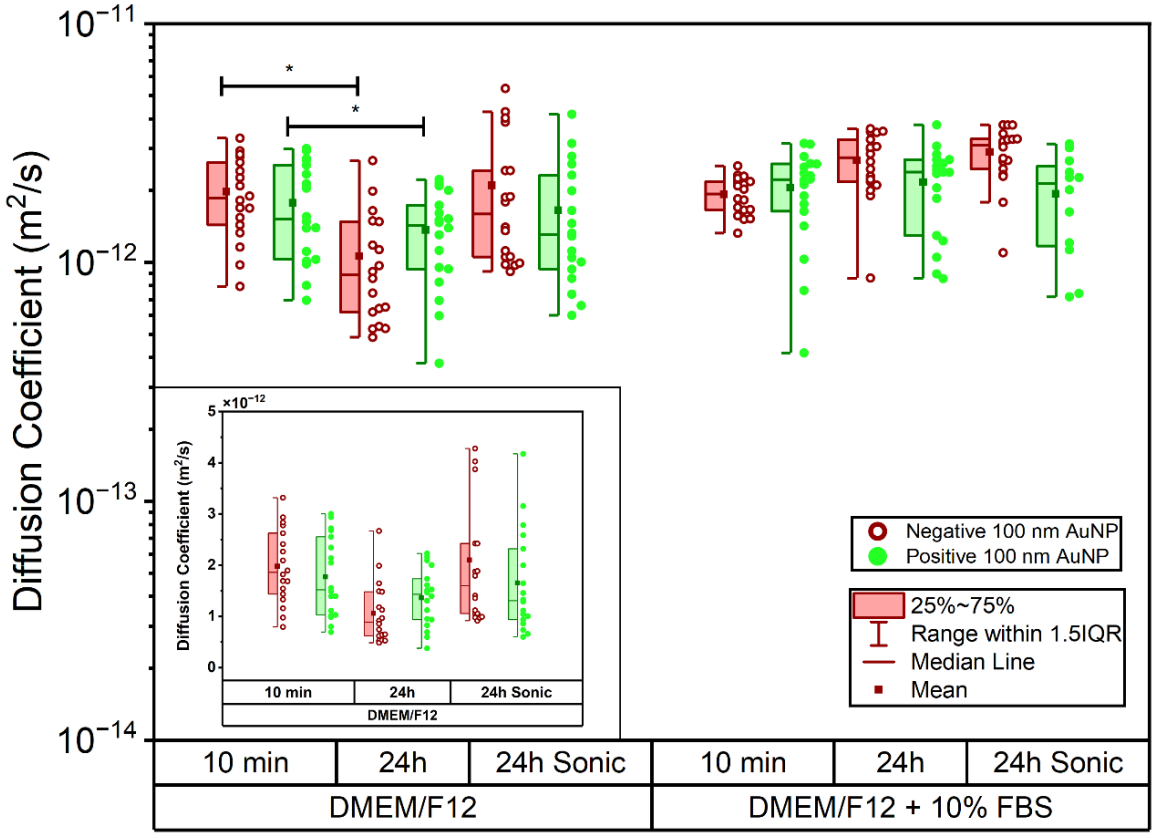


Fig.1 *Diffusion coefficient values of positively (green) and negatively (open red) charged 100 nm diameter gold nanoparticles in cell culture media with and without FBS, at two different incubation time points in the media (10 min and 24 h). At 24 h incubation, diffusion values for unsonicated samples prior tracking are labelled as '24h', and those with prior sonication after the 24h incubation period are labelled as '24h Sonic'.* $^{*}p \leq 0.05$, $^{**}p \leq 0.001$

Moreover, this explanation is supported by the effect of the sample sonication after the 24 h incubation and prior to the tracking analysis, shown in Figure 1 (24 h vs 24 h sonic). Here, there is no visual nor statistically significant difference between the diffusion coefficient values of the nanoparticles that have been incubated for 10 min compared to the particles that have been incubated for 24 h and sonicated in the serum-free media. This implies that the sonication process had successfully disrupted the particle-particle aggregates, retrieving a monodispersed suspension. Also, the sonication process had no effect on the nanoparticles incubated for 24 h in the protein-rich media, suggesting the formation of strong nanoparticle-protein interactions that cannot be disrupted through the sonication process.

The nanoparticle-protein interaction had been shown to happen for both negatively and positively charged nanoparticles and proven to be a charge independent process as previous studies had shown [40][54]. However, the dynamic process of specific protein adsorption can be affected by the surface charge of the nanoparticle, while positively-charged nanoparticles tend to undergo a higher protein adsorption of negative proteins, negatively surface charged nanoparticles adsorb fewer proteins. Over longer incubation times, this can be reflected in a more pronounced increase in diameter for positively-charged nanoparticles due to the larger amount of negatively charged proteins present in FBS (i.e. albumin) [54–56]. This is shown (Fig 1) through a higher rate of diffusion of negatively charge nanoparticles when incubated for 24 h in the serum rich media compared to the positively charged nanoparticles. This difference may be attributed to an increase in the hydrodynamic diameter of the positively-charged nanoparticles relative to their negatively-charged counterparts.

This system has proven to be effective at characterising the effect that the presence of proteins in the media has on stabilising nanoparticles through their interactions, and that this stabilisation is maintained over incubation time and unaffected by sonication.

Introduction of ARPE-19 cell monolayer effect on nanoparticle motion

After understanding the nanoparticle-protein interaction effect on the nanoparticles' diffusion, an ARPE-19 cell layer was introduced into the system. Figure 2 a) shows the successful growth of the ARPE-19 cell monolayer on a microscope glass coverslip comparing the bright field (left) and the caustics set-up (right) in the same focal plane on the optical microscope. In figure 2 b) a closer look, at the coverslip surface level, reveals the visible nanoparticles and the ARPE-19 cell-cell junctions, through the caustics image.

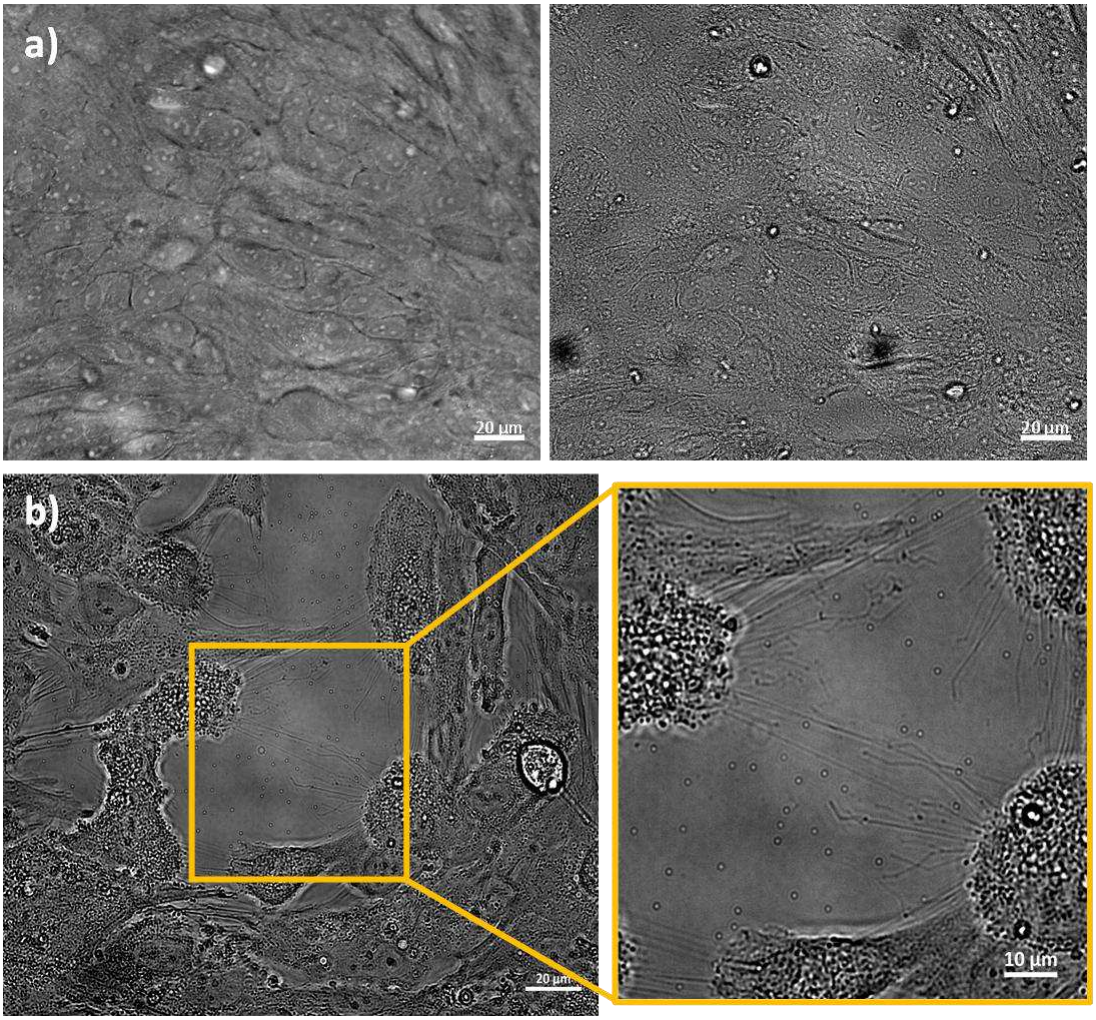


Fig. 2 *Visualisation of ARPE-19 cells grown on a glass microscope coverslip under a Zeiss Axio inverted optical microscope a) in bright field conditions (left) and with caustics settings (right); b) shows the cell-cell junctions between cells in the presence of nanoparticles sedimented on the microscope coverslip*

For the diffusion coefficient analysis, 100 nm diameter gold nanoparticles (separately positively and negatively surface charged) were tracked at 25 µm and at 50 µm above the cell monolayer. The experimental design is visually explained in figure 3. Initially, the surface of the cell monolayer was localised in the microscope as shown in figure 3 a) under bright field and b) with the caustics set-up, and here the microscope stage was set to z= 0 µm; from there, once 25 µm c) and 50 µm d) above the cells are reached the monolayer becomes out of focus but the caustics of the nanoparticles are easily identifiable and they were tracked for the diffusion analysis.

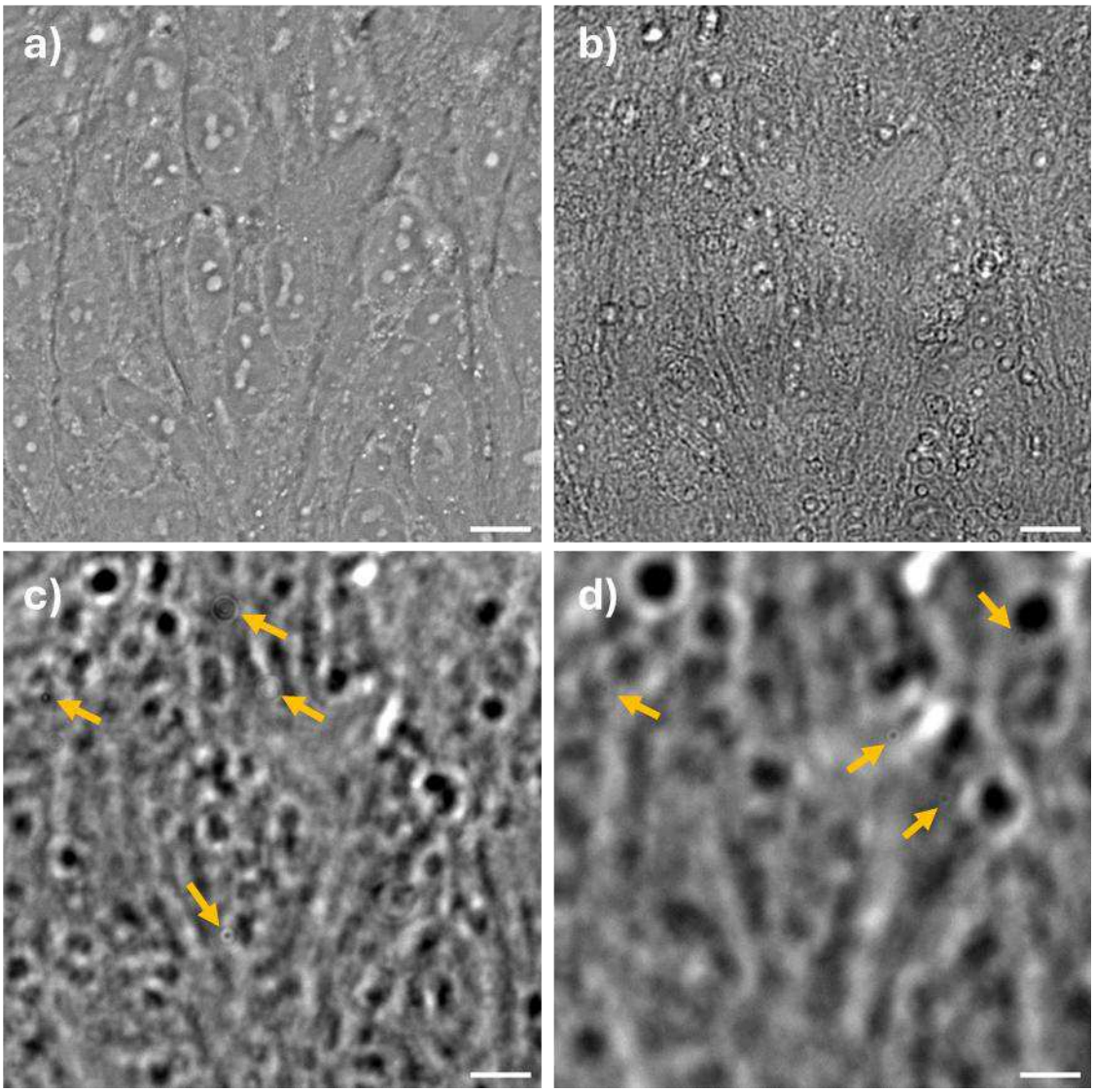


Fig. 3 *Microscopy images of ARPE-19 cells grown on a glass microscope coverslip incubated in DMEM/ F12 + 10% FBS with positively charged 100 nm diameter gold nanoparticles. a) Bright field images of the cells; b) same region of interest and focal plane with the caustics set-up; c) image take at 25 µm from the surface of the cell monolayer; d) image take at 50 µm from the surface of the cell monolayer. Yellow arrows show the caustic signatures of the 100 nm nanoparticles. Scale bar= 5 µm*

The results of the nanoparticles diffusion are shown in figure 4, which illustrates a wide spread of the diffusion values across both charges and independently of the presence of proteins. This reflects the increased complexity of the environment as a result of the introduction of the cell layer. However, the overall diffusion of positively-charged nanoparticles exhibited a decreasing trend compared to the negatively-charged particles; this charge penalty though was recovered in the protein-rich media. Probably, the presence of proteins had, once again, improved the stability of the particles, whereas the particles in the serum-free media were more prone to interact with biomolecules secreted from the cells.

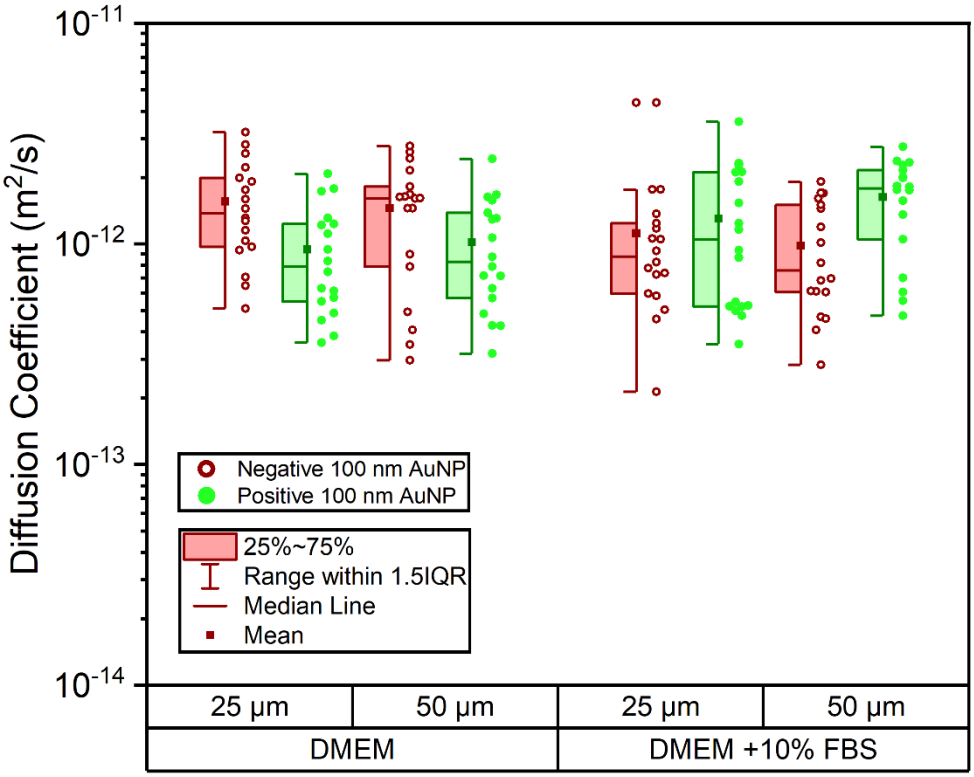


Fig. 4 *Diffusion coefficient values of positively (green) and negatively (open red) charged 100 nm diameter gold nanoparticles through cell culture media with and without FBS above the ARPE-19 cell monolayer, at two different distances from the cell layer, 25 µm and 50 µm*

The secretion of different factors from the ARPE-19 cells, such as lipoproteins, metabolic byproducts, signalling molecules, and even extracellular matrix (ECM) components, could have created a wider range of physicochemical properties in the particles, creating a cell-modified corona that had a direct impact on their diffusion [57]. Hence, the diffusion of the nanoparticles was shown to be governed by the protein-particle interactions in the absence of cells, but by heterogenous, cell-secreted biomolecules in their presence.

In addition, we can see that the distance from the cell layer had no impact on the diffusion, probably showing that there is no direct cellular interaction nor a thick extracellular matrix (ECM) secretion at this distance range and incubation times that could drag or hinder the nanoparticle transport. Here, the cell type and incubation time are two key parameters that could create a large variability on the effect of nanoparticle transport. For instance, the longer cells are incubated for, the higher deposition of ECM components (i.e. fibronectin and collagen), which can strongly affect the viscosity of the media surrounding the cell and, therefore hinder nanoparticle transport [58,59].

This establishes a proof of concept for the platforms' applicability in understanding nanoparticle motion and the influence of biological entities through the investigation of their diffusion coefficients, opening a wide range of possibilities for pharmacokinetic analysis.

Vitreous humour analogue optimisation

After establishing the effects of the ARPE-19 cell monolayer on nanoparticle transport, to complete the multicomponent model, the vitreous humour analogue was optimised to incorporate a physiologically relevant protein concentration, because it has been shown to be one of the most important parameters affecting the kinetics of the nanoparticles through cell culture media.

Agar and hyaluronic acid hydrogels previously proven to closely mimic animal-derived vitreous humour, form a more stable solution than the vitreous extraction from cadaveric eyes [18]. The 0.95 mg/mL and 0.7 mg/mL agar and hyaluronic acid concentration (respectively) was reported to be the hydrogel with the closest characteristics to mimic the vitreous humour extracted from porcine eyes [19]. To make this hydrogel more biologically relevant and to ensure the cytocompatibility with the ARPE-19 cell layer, foetal bovine serum (FBS) proteins were incorporated into the hydrogel and it was evaluated for toxicity.

Firstly, a qualitative analysis of the cytotoxicity was performed comparing the state of the cells before and after their incubation with the hydrogels. From figure 5, we can clearly see that the incubation with the AHA hydrogel alone had a toxic effect on the cells in both tested environments, the microscope coverslip a), and the bottom of the well b). This incubation with hydrogel only, made the cells detach and acquire a round morphology characteristic of dead cells, compared to the healthy cobblestone-like monolayer from the image at the top (pretreated, figure 5). However, the 50:50 mix of AHA hydrogel with DMEM/F12 +10%FBS maintained the viability and structure of the cell monolayer. More interestingly, no difference can be appreciated from figure 5 a) and b) which validates the seeding on glass coverslips as a method that maintains the confluent monolayer of ARPE-19 cells.

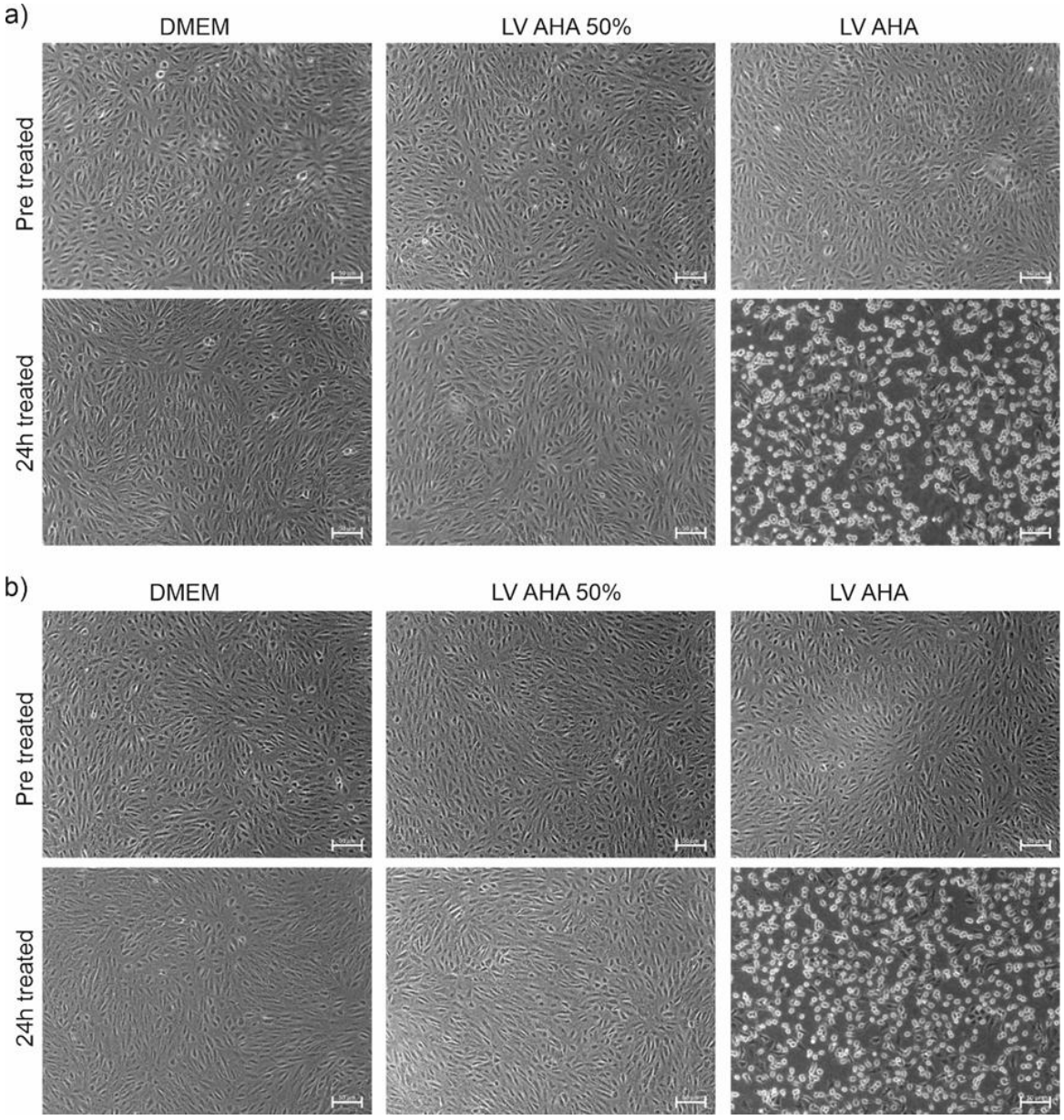


Fig. 5 *Optical microscopy images of ARPE-19 cells incubated for 48 h to achieve a confluent cell monolayer on glass microscope coverslips (in a 6-well plate), showing the effect of 24 h incubation with 50% AHA hydrogel in DMEM/F12 +10% FBS and AHA hydrogel alone compared to the control (DMEM/F12 with 10% FBS). a) Shows the results when the cells were cultured on glass microscope coverslips and b) when the cells were directly seeded in the 6-well plate. Scale bar= 50 µm*

Secondly, the AHA hydrogel: DMEM (10% FBS) ratio was optimised through the same qualitative method. As illustrated in figure 6, the characteristic cobblestone morphology of the ARPE-19 cells was preserved at an AHA hydrogel concentration of 80% (v/v). Cytotoxicity became apparent only when the media decreased to 10% (v/v); at this threshold, significant cell detachment and changes in cell morphology was observed.

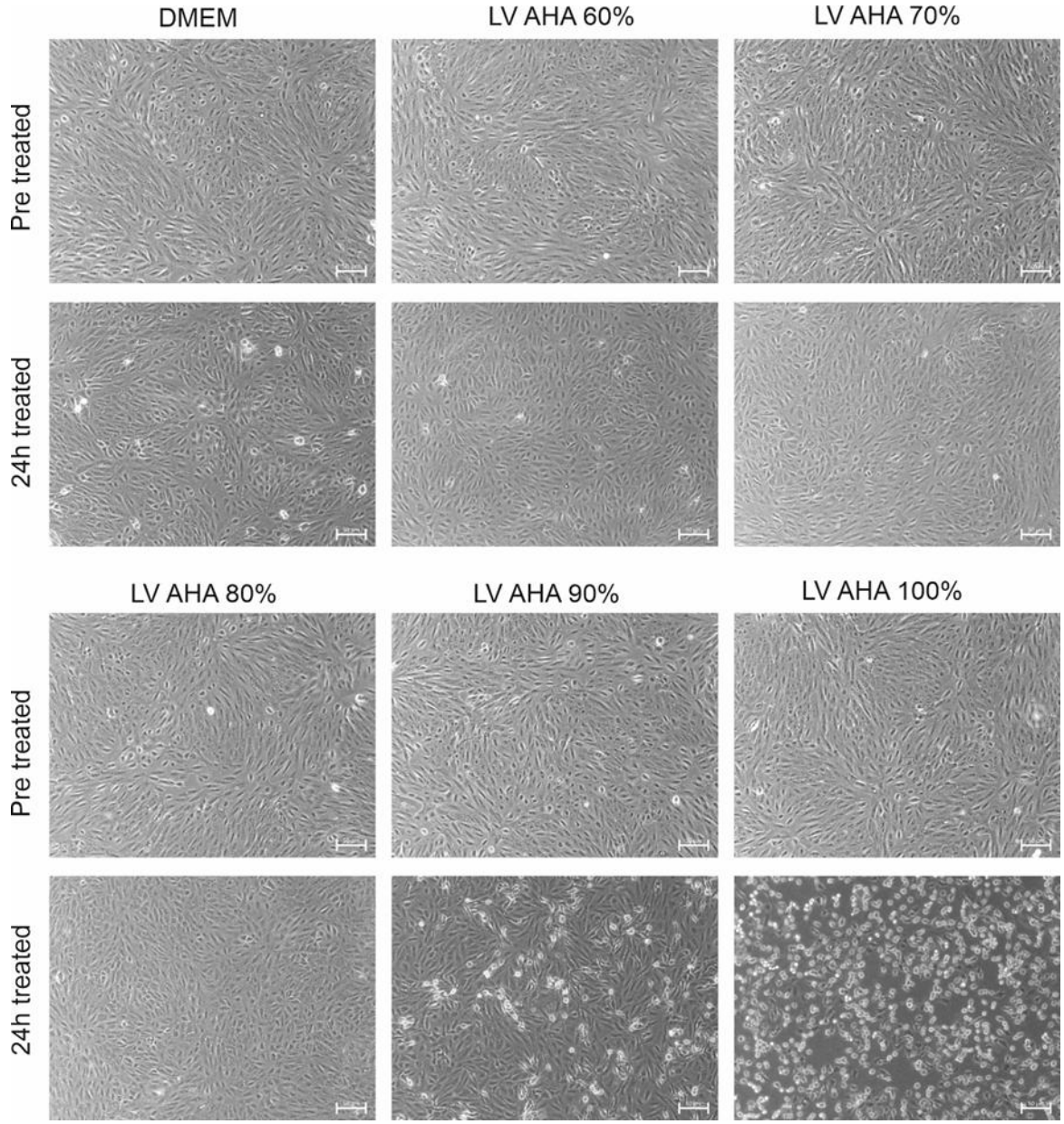


Fig. 6 *Optical microscopy images of ARPE-19 cells incubated for 48 h to achieve a confluent cell monolayer on glass microscope coverslips (in a 6-well plate). Showing pre-treated and 24 h incubated with different concentrations of agar and hyaluronic acid (AHA) hydrogel in DMEM/F12 with 10% FBS. Scale bar= 50 µm*

Finally, the ARPE-19 cell metabolic activity was assessed using the resazurin assay following exposure to different ratios of AHA hydrogel and DMEM/F12 +10% FBS (DMEM alone, 60:40, 70:30, 80:20, 90:10, and AHA hydrogel alone). As shown in figure 7, where the fluorescence intensity has been used as a proxy for cell viability and normalised to the untreated control (full media), no reduction in the metabolic activity was shown for the 90% hydrogel concentration, and the hydrogel only showed toxicity in the cell monolayer when used on its own. This difference between the visual and quantifiable methods might be due to the 2-hour incubation with full media in the resazurin assay, which could have led to a recovery in the metabolic activity of the cells incubated with the 90% (v/v) AHA hydrogel. Therefore, the use of 80% (v/v) concentration is

here considered a safe approach to preserve all cell functions and a stable monolayer throughout the microscope coverslip. Moreover, this concentration (2% FBS) aligns with the simulated concentrations of proteins present in a healthy vitreous humour, making the model a more accurate representation of the nanoparticle-protein interaction [60] .

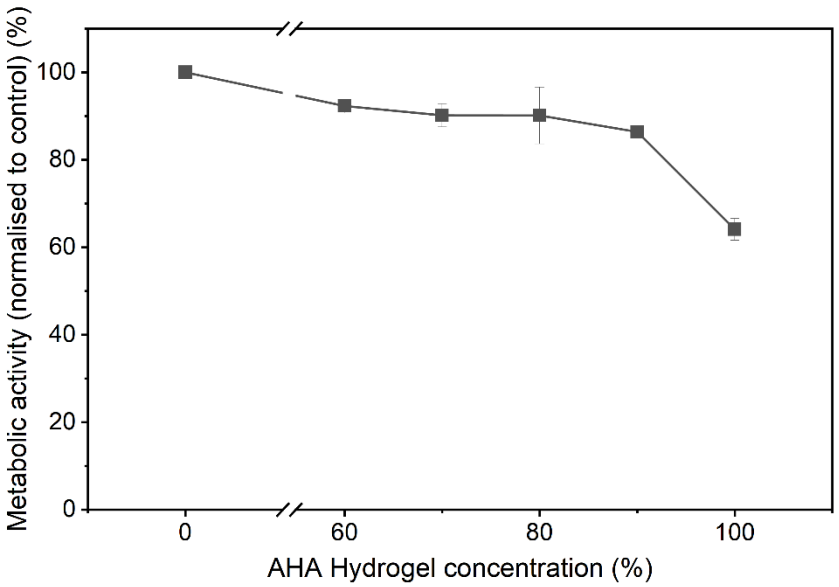


Fig. 7 *ARPE-19 cells metabolic activity assessment through the Resazurin assay, after their exposure to different concentrations of the agar and hyaluronic acid (AHA) hydrogel in cell culture media (DMEM/F12 + 10% FBS). Values of metabolic activity were normalised to the control, 0% AHA hydrogel (DMEM/F12 + 10% FBS), and presented as %. The error bars represent ±1SD*

It is worth noting that vitreous protein concentration can significantly fluctuate with different diseases, such as diabetic retinopathy (DR) and age-related macular degeneration (AMD) [60,61]. Similarly, ageing and disease progression induce structural and mechanical degradation of the vitreous humour, characterised by the liquefaction [15]. These biochemical and rheological changes can directly impact the intravitreal drug delivery. Consequently, the capacity to tune these parameters, by optimising agar and hyaluronic acid concentrations and modulating protein content in this existing analogue presented here, enables the development of potential pathophysiological vitreous analogues, facilitating a more accurate, disease-specific model to optimise drug delivery to the retina.

Multicomponent in vitro eye model for nanoparticle transport analysis

The optimised vitreous analogue based on agar and hyaluronic acid hydrogel (80%) with DMEM/F12 +10% FBS (20%) was injected separately with positively and negatively surface charged 100 nm diameter gold nanoparticles, the mix was aliquoted into a microscope slide and sealed with a microscope coverslip with the ARPE-19 cell monolayer. The nanoparticles were also tracked at two different distances (25 µm and 50 µm) from the cell layer.

The results in figure 8 show that when nanoparticles are diffusing across the vitreous analogue, independently of the ARPE-19 cell presence, a wide range of diffusion coefficient values were recorded. These figures were found to cover three orders of magnitude ranging from values of the order of 10^{-12} to values of the order of 10^{-15}, agreeing with our previous research in agar and hyaluronic acid hydrogels [19,62]. This suggests that the nanoparticles that present diffusion values between 10^{-12} to 10^{-13} are diffusing in an aqueous phase, according with the values recorded in the cell culture media, and for those diffusing at the order of 10^{-14} and 10^{-15} are expected to be experiencing some interaction with a gel matrix.

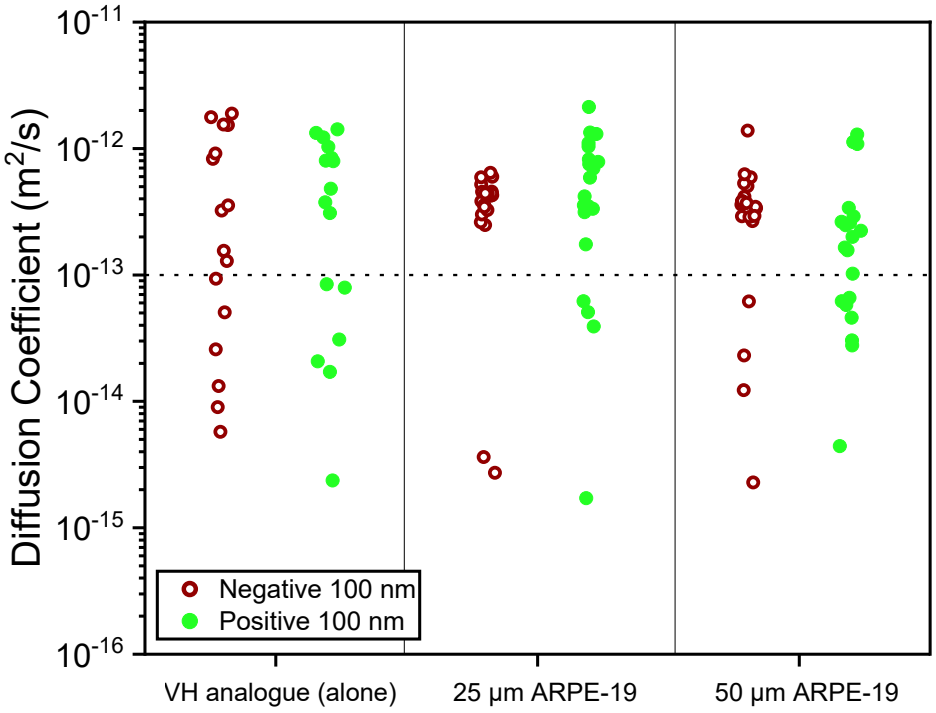


Fig. 8 *Diffusion coefficient values of positively (green) and negatively (open red) charged 100 nm diameter gold nanoparticles in the vitreous humour analogue alone (left), in the vitreous humour analogue above 25 µm of the ARPE-19 cell layer (centre), and in the vitreous humour analogue above 50 µm of the ARPE-19 cell layer (right). The dotted line refers to the approximate (10^{-13} m^2/s) transition between the aqueous (above) and gel (below) phases of the hydrogel*

Furthermore, the strong correlation between the diffusion coefficient values and the area of the convex hull enclosing the path followed by the particle, shown in Figure 9, corroborates that higher values of diffusion were directly related to particles diffusing further away from their starting point, therefore, more freely in an aqueous phase. While lower values of nanoparticle diffusion were directly related to a short excursion from their starting point, showing that their interaction with the gel matrix prevented their movement. This presence of different phases

affecting the nanoparticle transport in the vitreous humour analogue shows its potential to model the real composition of the vitreous humour, which is also composed of two different phases, an aqueous vitreous humour and a gel vitreous humour. This emphasises the possibility of developing disease models by modulating the ratio of the aqueous and gel phases in the synthesis of the vitreous humour analogue [63,64].

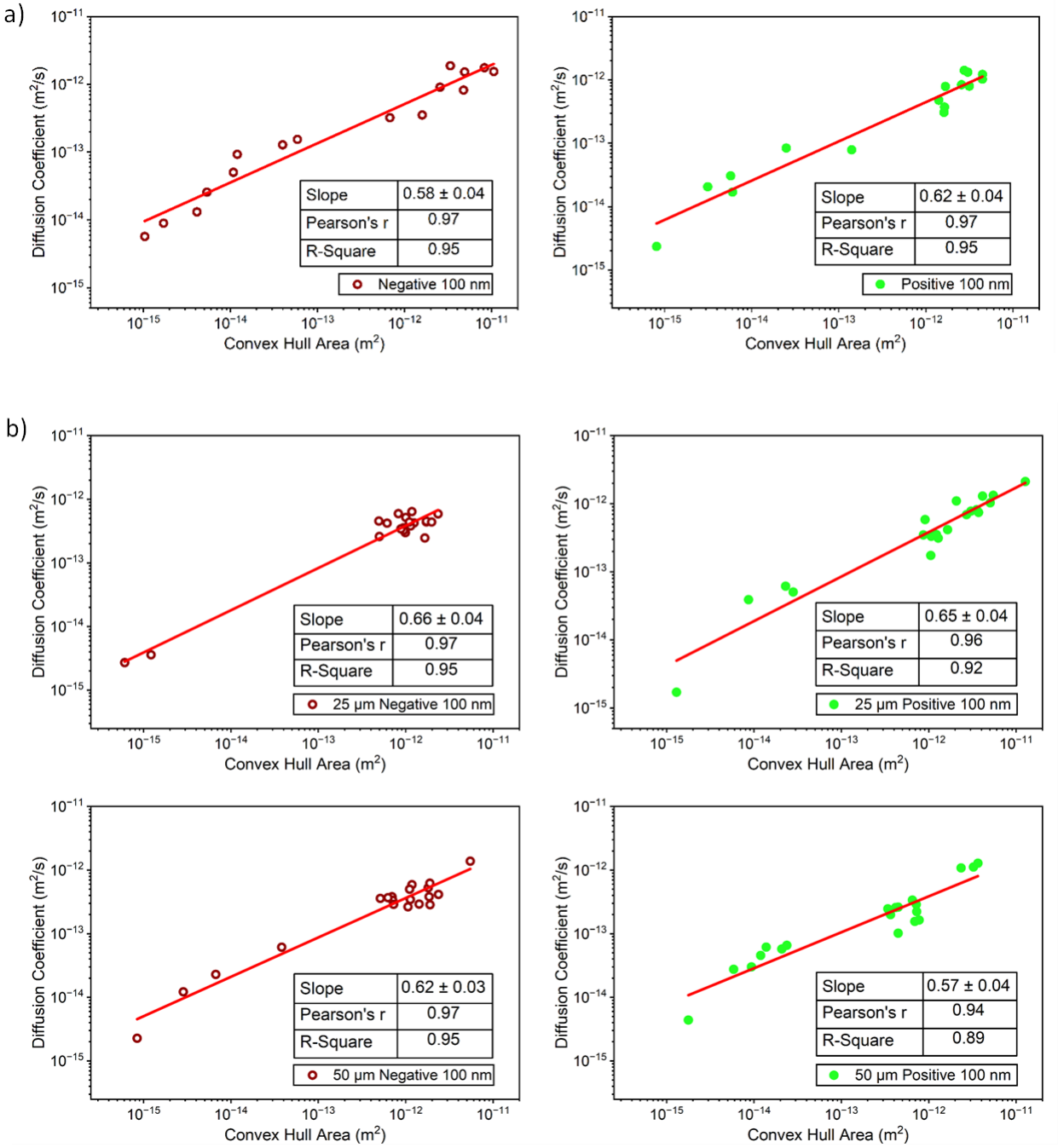


Fig. 9 *Correlation between the diffusion coefficient values of positive (green - right) and negative (open red - left) 100 nm diameter gold nanoparticles and the area of the convex hull of each nanoparticle trail of motion, in a) the synthetic in vitro vitreous humour analogue and b) the vitreous analogue above the ARPE-19 cell layer, above 25 µm (top) and above 50 µm bottom)*

The frequency distribution of the diffusion coefficients shown in figure 10 helps to visualise the distribution of the nanoparticles in the vitreous humour analogue. The nanoparticle diffusion across the different phases of the vitreous humour analogue was shown to have a uniform distribution across a range of diffusion values (10^{-12} to 10^{-15}) in a charge independent manner when the nanoparticles were tracked in the vitreous humour analogue alone. However, this pattern was found to drastically change when the ARPE-19 cell layer was introduced, where a relatively high number of nanoparticles were found to be diffusing in the aqueous phase. This shift was found to be dependent on both surface charge and distance from the ARPE-19 cells. Where on one hand, 90% of the negatively-charged nanoparticles and 80% of the positively-charged nanoparticles above 25 μm were found to be diffusing in an aqueous phase. On the other hand, 80% of negatively-charged nanoparticles and only 60% of the positively-charged nanoparticles showed an aqueous-based diffusion above 50 μm from the cell layer. Hence, implying there is an aqueous-based interface surrounding the cell layer, which becomes increasingly gel-based with distance away from the monolayer of cells. Moreover, the migration of nanoparticles across the analogue into the interface surrounding the cell apparently shows the capability of these nanoformulations to travel across the analogue and reach the targeted tissue.

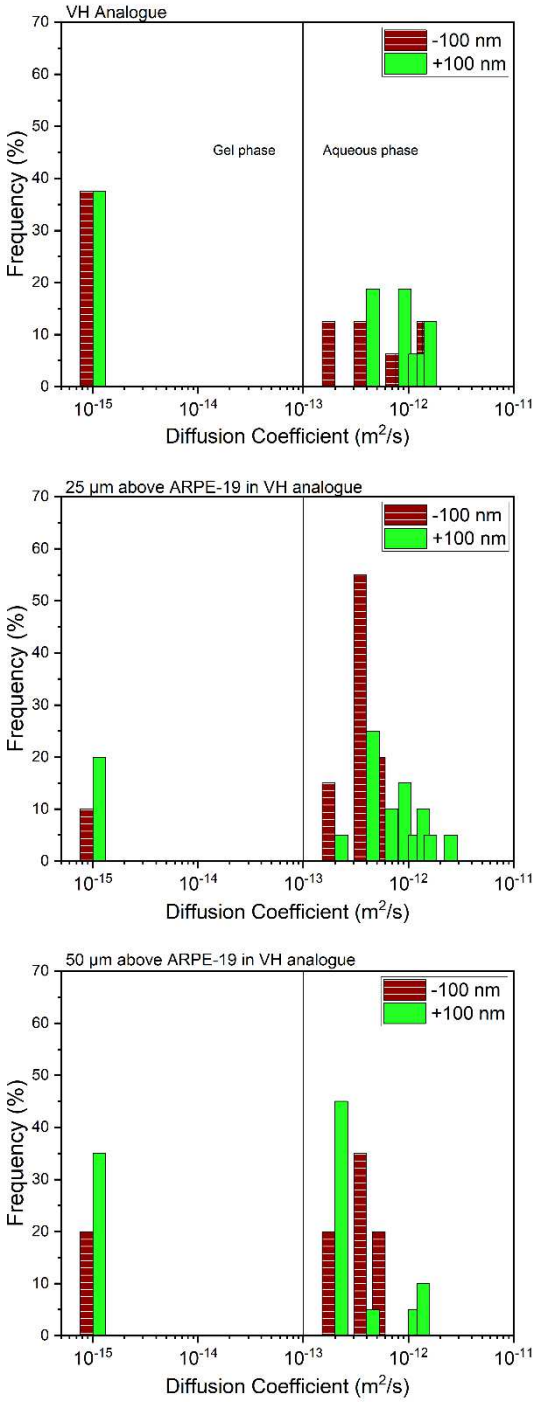


Fig. 8 *Frequency plots of the distribution of diffusion coefficient values for the positively (green) and negatively (red-dashed) charged 100 nm diameter gold nanoparticles. Comparing the vitreous humour (VH) analogue alone (top) and the multicomponent model composed of the vitreous analogue and the ARPE-19 cell monolayer at a distance of 25 µm (middle) and at 50 µm from the cell layer (bottom). The vertical line at 10^{-13} (m^2/s) represents the separation between the nanoparticles diffusing in the gel (left) and the aqueous (right) phases of the VH analogue*

1

Conclusion

Understanding pharmacokinetic properties is key for successfully designing nanoparticle-based drug delivery systems across diverse biomedical and biomaterial applications. Hence, the aim of our multicomponent model is to investigate two major factors affecting nanoparticle transport: dynamic transformation due to their interaction with proteins, and their distribution/ interaction with a complex hydrogel matrix.

The platform presented here, demonstrated using a vitreous humour analogue and an ARPE-19 cell monolayer coupled with a label-free microscopy platform as an example, has successfully uncovered that the nanoparticle-protein interaction is independent of charge. It has been used to observe the stabilisation of the nanoparticles in protein-rich media when compared to serum deprived DMEM. The introduction of the cell monolayer increased the biological complexity of the media through the potential cell secretion of biomolecules that interacted with the nanoparticles thus masking the protein interactions, amplifying the dynamic nature of the interactions, and increasing the variability.

Moreover, the diffusion of the nanoparticles exhibited a bimodal distribution across the hydrogel analogue, where nanoparticles appeared to diffuse either through a distinct aqueous-like or gel-like microenvironment. This set-up successfully replicated the dual-phase characteristics of the vitreous humour, demonstrating the platform's capacity to model heterogeneous soft matter matrices. This distribution was heavily impacted by the introduction of cells, where the distance from the monolayer and the nanoparticle surface charge seemed to be key features influencing the type of diffusion. As the great majority of the nanoparticles exhibited high diffusion values at 25 µm from the cell layer, this suggests the presence of an aqueous-based interfacial boundary layer surrounding the cell monolayer.

In summary, the developed platform serves as a highly adaptable, reproducible and cost-effective tool for the optimisation of nanoparticle-based drug delivery systems and hydrogel-cell interface modelling. The easily tuneable feature of the platform gives it the potential to replicate diverse clinical environments, including variable matrix degradation states, disease-specific protein profiles, alternative cell-line selection, and custom temporal dynamics.

Acknowledgements

We would like to acknowledge the ARPE-19 cell line expertise of Abigail Christie. This work was supported by the Doctoral Network in Technologies for Healthy Ageing; and the Engineering and Physical Sciences Research Council [grant numbers EP/R024839/1; EP/S012265/1].

Author contributions

MLL performed data curation, analysis, and writing of first draft; VK provided the ARPE-19 cells, advised on cell culture and vitreous humour analogues, EAP advised on data analysis and microscopy technique, JMC was the PI and grant holder. All authors contributed to manuscript editing and writing.

Declarations

VK is a member of the editorial board of the journal *In vitro models* otherwise the authors declare no competing interests.

Data Availability

The datasets generated and/or analysed during the current study are available in the [DataCat: The Research Data Catalogue] repository, [DOI: 10.17638/datacat.liverpool.ac.uk/3069]

References

1. Parveen S, Bozal SB, Pober JS, Saltzman WM. Nanoparticle-hydrogel composites for precision medicine. Cell Biomaterials [Internet]. Cell Press; 2026 [cited 2026 Jul 31];100372. https://doi.org/10.1016/J.CELBIO.2026.100372

2. Radermacher C, Rohde A, Kucikas V, Buhl EM, Wein S, Jonigk D, et al. Various Hydrogel Types as a Potential In Vitro Angiogenesis Model. Gels [Internet]. Multidisciplinary Digital Publishing Institute (MDPI); 2024 [cited 2026 Jul 31];10:820. https://doi.org/10.3390/GELS10120820/S1

3. Tanaka M, Nakahata M, Linke P, Kaufmann S. Stimuli-responsive hydrogels as a model of the dynamic cellular microenvironment. Polymer Journal 2020 52:8 [Internet]. Nature Publishing Group; 2020 [cited 2026 Jul 31];52:861–70. https://doi.org/10.1038/s41428-020-0353-6

4. Alfonsetti M, Castelli V, D'angelo M, Benedetti E, Allegretti M, Barboni B, et al. Looking for in vitro models for retinal diseases. Int. J. Mol. Sci. MDPI; 2021. https://doi.org/10.3390/ijms221910334

5. Dujardin C, Habeler W, Monville C, Letourneur D, Simon-Yarza T. Advances in the engineering of the outer blood-retina barrier: From in-vitro modelling to cellular therapy. Bioact. Mater. KeAi Communications Co.; 2024. p. 151–77. https://doi.org/10.1016/j.bioactmat.2023.08.003

6. Gensheimer T, Veerman D, van Oosten EM, Segerink L, Garanto A, van der Meer AD. Retina-on-chip: engineering functional in vitro models of the human retina using organ-on-chip technology. Lab Chip. Royal Society of Chemistry; 2025. p. 996–1014. https://doi.org/10.1039/d4lc00823e

7. Eiraku M, Takata N, Ishibashi H, Kawada M, Sakakura E, Okuda S, et al. Self-organizing optic-cup morphogenesis in three-dimensional culture. Nature. 2011;472:51–8. https://doi.org/10.1038/nature09941

8. Kurzawa-Akanbi M, Tzoumas N, Corral-Serrano JC, Guarascio R, Steel DH, Cheetham ME, et al. Pluripotent stem cell-derived models of retinal disease: Elucidating pathogenesis, evaluating novel treatments, and estimating toxicity. Prog. Retin. Eye Res. Elsevier Ltd; 2024. https://doi.org/10.1016/j.preteyeres.2024.101248

9. Bohley M, Dillinger AE, Tamm ER, Goepferich A. Targeted drug delivery to the retinal pigment epithelium: Untapped therapeutic potential for retinal diseases. Drug Discov Today [Internet]. Elsevier Ltd; 2022;27:2497–509. https://doi.org/10.1016/j.drudis.2022.05.024

10. Jiang S, Franco YL, Zhou Y, Chen J. Nanotechnology in retinal drug delivery. Int J Ophthalmol. 2018;11:1038–44. https://doi.org/10.18240/ijo.2018.06.23

11. Wang R, McClard CK, Laswell S, Mahmoudzadeh R, Salabati M, Ammar M, et al. Quantifying burden of intravitreal injections: questionnaire assessment of life impact of treatment by intravitreal injections (QUALITII). BMJ Open Ophthalmol [Internet]. BMJ Publishing Group; 2022 [cited 2026 Feb 5];7:e001188. https://doi.org/10.1136/BMJOPHTH-2022-001188

12. Lee J, Rhee Y-S. Ophthalmic dosage forms for drug delivery to posterior segment. J Pharm Investig [Internet]. 2022 [cited 2024 Jan 12];52:161–73. https://doi.org/10.1007/s40005-021-00554-8

13. Peynshaert K, Devoldere J, De Smedt SC, Remaut K. In vitro and ex vivo models to study drug delivery barriers in the posterior segment of the eye. Adv Drug Deliv Rev [Internet]. Elsevier B.V.; 2018;126:44–57. https://doi.org/10.1016/j.addr.2017.09.007

14. Kicková E, Sadeghi A, Puranen J, Tavakoli S, Sen M, Ranta VP, et al. Pharmacokinetics of pullulan–dexamethasone conjugates in retinal drug delivery. Pharmaceutics. 2022;14. https://doi.org/10.3390/pharmaceutics14010012

15. Mishra D, Gade S, Glover K, Sheshala R, Singh TRR. Vitreous Humor: Composition, Characteristics and Implication on Intravitreal Drug Delivery. Curr Eye Res [Internet]. Taylor & Francis; 2023;48:208–18. https://doi.org/10.1080/02713683.2022.2119254

16. Penkova A, Moats R, Humayun MS, Fraser S, Sadhal SS. Diffusive Transport in the Vitreous Humor: Experimental and Analytical Studies. J Heat Transfer. 2019;141:1–11. https://doi.org/10.1115/1.4042297

17. Awwad S, Lockwood A, Brocchini S, Khaw PT. The PK-Eye: A Novel in Vitro Ocular Flow Model for Use in Preclinical Drug Development. J Pharm Sci [Internet]. Elsevier Masson SAS; 2015;104:3330–42. https://doi.org/10.1002/jps.24480

18. Thakur SS, Shenoy SK, Suk JS, Hanes JS, Rupenthal ID. Validation of hyaluronic acid-agar-based hydrogels as vitreous humor mimetics for in vitro drug and particle migration evaluations. European Journal of Pharmaceutics and Biopharmaceutics [Internet]. Elsevier; 2020;148:118–25. https://doi.org/10.1016/j.ejpb.2020.01.008

19. Lorenzo Lopez M, Kearns VR, Curran JM, Patterson EA. Diffusion of nanoparticles in heterogeneous hydrogels as vitreous humour in vitro substitutes. Sci Rep [Internet]. Nature Publishing Group UK; 2024;14:1–13. https://doi.org/10.1038/s41598-024-68267-0

20. Kang-Mieler JJ, Rudeen KM, Liu W, Mieler WF. Advances in ocular drug delivery systems. Eye (Basingstoke). Springer Nature; 2020. p. 1371–9. https://doi.org/10.1038/s41433-020-0809-0

21. Meza-Rios A, Navarro-Partida J, Armendariz-Borunda J, Santos A. Therapies Based on Nanoparticles for Eye Drug Delivery. Ophthalmol Ther [Internet]. Springer Healthcare; 2020;9:401–14. https://doi.org/10.1007/s40123-020-00257-7

22. Cioffi CL. Drug Delivery Challenges and Novel Therapeutic Approaches for Retinal Diseases. 2020.

23. Park SJ. Protein–nanoparticle interaction: Corona formation and conformational changes in proteins on nanoparticles. Int J Nanomedicine. 2020;15:5783–802. https://doi.org/10.2147/IJN.S254808

24. Monopoli MP, Åberg C, Salvati A, Dawson KA. Biomolecular coronas provide the biological identity of nanosized materials. Nat Nanotechnol. Nature Publishing Group; 2012;7:779–86. https://doi.org/10.1038/nnano.2012.207

25. Nguyen VH, Lee BJ. Protein corona: A new approach for nanomedicine design. Int J Nanomedicine. 2017;12:3137–51. https://doi.org/10.2147/IJN.S129300

26. Capjak I, Goreta SŠ, Jurašin DD, Vrček IV. How protein coronas determine the fate of engineered nanoparticles in biological environment. Arh Hig Rada Toksikol. 2017;68:245–53. https://doi.org/10.1515/aiht-2017-68-3054

27. Charbgoo F, Nejabat M, Abnous K, Soltani F, Taghdisi SM, Alibolandi M, et al. Gold nanoparticle should understand protein corona for being a clinical nanomaterial. Journal of Controlled Release [Internet]. Elsevier; 2018;272:39–53. https://doi.org/10.1016/j.jconrel.2018.01.002

28. Tavakoli S, Kari OK, Turunen T, Lajunen T, Schmitt M, Lehtinen J, et al. Diffusion and Protein Corona Formation of Lipid-Based Nanoparticles in the Vitreous Humor: Profiling and Pharmacokinetic Considerations. Mol Pharm. 2021;18:699–713. https://doi.org/10.1021/acs.molpharmaceut.0c00411

29. Total protein: MedlinePlus Medical Encyclopedia [Internet]. [cited 2026 Jan 19]. https://medlineplus.gov/ency/article/003483.htm. Accessed 19 Jan 2026

30. Lieto K, Skopek R, Lewicka A, Stelmasiak M, Klimaszewska E, Zelent A, et al. Looking into the Eyes—In Vitro Models for Ocular Research. Int. J. Mol. Sci. MDPI; 2022. https://doi.org/10.3390/ijms23169158

31. Aotaki-Keen AE, Putkey FR, Hjelmeland ??? L M. ARPE-19, A Human Retinal Pigment Epithelial Cell Line with Differentiated Properties. Exp. Eye Res. 1996.

32. D'Amico AG, Maugeri G, Rasà D, Federico C, Saccone S, Lazzara F, et al. NAP modulates hyperglycemic–inflammatory event of diabetic retina by counteracting outer blood retinal barrier damage. J Cell Physiol. Wiley-Liss Inc.; 2019;234:5230–40. https://doi.org/10.1002/jcp.27331

33. Jamshidi M, Jamshidi N, Falamaki C. Nanoparticle Tracking Analysis: Enhanced Detection of Transparent Materials. Particle and Particle Systems Characterization. John Wiley and Sons Inc; 2023;40. https://doi.org/10.1002/ppsc.202200173

34. Zhang C, Tian Z, Chen R, Rowan F, Qiu K, Sun Y, et al. Advanced imaging techniques for tracking drug dynamics at the subcellular level. Adv Drug Deliv Rev [Internet]. Elsevier B.V.; 2023;199:114978. https://doi.org/10.1016/j.addr.2023.114978

35. Snipstad S, Hak S, Baghirov H, Sulheim E, Mørch Ý, Lélu S, et al. Labeling nanoparticles: Dye leakage and altered cellular uptake. Cytometry Part A. 2017;91:760–6. https://doi.org/10.1002/cyto.a.22853

36. Thomsen T, Ayoub AB, Psaltis D, Klok HA. Fluorescence-Based and Fluorescent Label-Free Characterization of Polymer Nanoparticle Decorated T Cells. Biomacromolecules. 2021;22:190–200. https://doi.org/10.1021/acs.biomac.0c00969

37. Jensen EC. Use of Fluorescent Probes: Their Effect on Cell Biology and Limitations. Anatomical Record. Blackwell Publishing Inc.; 2012. p. 2031–6. https://doi.org/10.1002/ar.22602

38. Bailey MLP, Pratt SE, Hinrichsen M, Zhang Y, Bewersdorf J, Regan LJ, et al. Uncovering diffusive states of the yeast membrane protein, Pma1, and how labeling method can change diffusive behavior. European Physical Journal E [Internet]. 2023 [cited 2024 Jan 12];46:42. https://doi.org/10.1140/epje/s10189-023-00301-x

39. Giorgi F, Macko P, Curran JM, Whelan M, Worth A, Patterson EA. Settling dynamics of nanoparticles in simple and biological media. R Soc Open Sci. 2021;8. https://doi.org/10.1098/rsos.210068

40. Schleyer G, Patterson EA, Curran JM. Label free tracking to quantify nanoparticle diffusion through biological media. Sci Rep. Nature Research; 2024;14. https://doi.org/10.1038/s41598-024-69506-0

41. Patterson EA, Whelan MP. Tracking nanoparticles in an optical microscope using caustics. Nanotechnology. 2008;19. https://doi.org/10.1088/0957-4484/19/10/105502

42. Patterson EA, Whelan MP. Optical signatures of small nanoparticles in a conventional microscope. Small. 2008;4:1703–6. https://doi.org/10.1002/smll.200800703

43. Tinevez JY, Perry N, Schindelin J, Hoopes GM, Reynolds GD, Laplantine E, et al. TrackMate: An open and extensible platform for single-particle tracking. Methods [Internet]. The Author(s); 2017;115:80–90. https://doi.org/10.1016/j.ymeth.2016.09.016

44. Radenovic A. Brownian Motion and Single Particle Tracking. LbenEpflCh [Internet]. 2005;1–23. http://lben.epfl.ch/files/content/sites/lben/files/users/179705/Brownian Motion Handout.pdf

45. Einstein A. Investigations O N the Theory .of ,the Brownian Movement R. F Ü R T H Translated By. Dover, New York. 1956;

46. Douglas Mcllroy M, Bentley JL, Faust MG, Preparata FP. Technical Notes Programming Techniques and Data Structures Approximation Algorithms for Convex Hulls. 1982.

47. Masse F, Ouellette M, Lamoureux G, Boisselier E. Gold nanoparticles in ophthalmology. Med Res Rev. 2019;39:302–27. https://doi.org/10.1002/med.21509

48. Dykman L, Khlebtsov B, Khlebtsov N. Drug delivery using gold nanoparticles. Adv. Drug Deliv. Rev. Elsevier B.V.; 2025. https://doi.org/10.1016/j.addr.2024.115481

49. Jain P, Pawar RS, Pandey RS, Madan J, Pawar S, Lakshmi PK, et al. In-vitro in-vivo correlation (IVIVC) in nanomedicine: Is protein corona the missing link? Biotechnol Adv. 2017;35:889–904. https://doi.org/10.1016/j.biotechadv.2017.08.003

50. Hirsh SL, McKenzie DR, Nosworthy NJ, Denman JA, Sezerman OU, Bilek MMM. The Vroman effect: Competitive protein exchange with dynamic multilayer protein aggregates. Colloids Surf B Biointerfaces. 2013;103:395–404. https://doi.org/10.1016/j.colsurfb.2012.10.039

51. Gentili D, Ori G. Reversible assembly of nanoparticles: theory, strategies and computational simulations. Nanoscale. Royal Society of Chemistry; 2022. p. 14385–432. https://doi.org/10.1039/d2nr02640f

52. Akhter MH, Khalilullah H, Gupta M, Alfaleh MA, Alhakamy NA, Riadi Y, et al. Impact of protein corona on the biological identity of nanomedicine: Understanding the fate of nanomaterials in the biological milieu. Biomedicines. MDPI; 2021. https://doi.org/10.3390/biomedicines9101496

53. Lee YK, Choi EJ, Webster TJ, Kim SH, Khang D. Effect of the protein corona on nanoparticles for modulating cytotoxicity and immunotoxicity. Int. J. Nanomedicine. Dove Medical Press Ltd.; 2014. p. 97–113. https://doi.org/10.2147/IJN.S72998

54. Barbalinardo M, Chiarini F, Teti G, Paganelli F, Mercadelli E, Bartoletti A, et al. Surface Charge Overrides Protein Corona Formation in Determining the Cytotoxicity, Cellular Uptake, and Biodistribution of Silver Nanoparticles. ACS Appl Bio Mater. American Chemical Society; 2025;8:5032–43. https://doi.org/10.1021/acsabm.5c00392

55. Hühn D, Kantner K, Geidel C, Brandholt S, De Cock I, Soenen SJH, et al. Polymer-Coated Nanoparticles Interacting with Proteins and Cells: Focusing on the Sign of the Net Charge. ACS Nano [Internet]. American Chemical Society; 2013 [cited 2026 Jan 27];7:3253–63. https://doi.org/10.1021/NN3059295

56. Liu X, Huang N, Li H, Jin Q, Ji J. Surface and Size Effects on Cell Interaction of Gold Nanoparticles with Both Phagocytic and Nonphagocytic Cells. Langmuir [Internet]. American Chemical Society; 2013 [cited 2026 Jan 27];29:9138–48. https://doi.org/10.1021/LA401556K

57. Ji A, Hamid A, Andrabi SAH, Haq E ul, Tombuloglu H. Interaction of nanoparticles with biomolecules. Molecular Impacts of Nanoparticles on Plants and Algae [Internet]. Academic Press; 2024 [cited 2026 Jan 27];143–57. https://doi.org/10.1016/B978-0-323-95721-2.00008-7

58. Liu FD, Zeiger AS, Van Vliet KJ. Time-Dependent Extracellular Matrix Organization and Secretion from Vascular Endothelial Cells due to Macromolecular Crowding. MRS Online Proceedings Library (OPL) [Internet]. Cambridge University Press; 2014 [cited 2026 Jan 19];1623:mrsf13-1623-f02-10. https://doi.org/10.1557/OPL.2014.121

59. Kearns VR, Jack Tasker •, Zhuola •, Riaz Akhtar •, Akash Bachhuka •, Krasimir Vasilev •, et al. The formation of a functional retinal pigment epithelium occurs on porous polytetrafluoroethylene substrates independently of the surface chemistry. J Mater Sci: Mater Med. 2017;28:124. https://doi.org/10.1007/s10856-017-5926-3

60. Loukovaara S, Nurkkala H, Tamene F, Gucciardo E, Liu X, Repo P, et al. Quantitative Proteomics Analysis of Vitreous Humor from Diabetic Retinopathy Patients. J Proteome Res [Internet]. American Chemical Society; 2015 [cited 2026 Jan 27];14:5131–43. https://doi.org/10.1021/ACS.JPROTEOME.5B00900

61. Kose H, Ozkan B, Kanli A, Karabas L V., Akpinar G, Kasap M, et al. Evaluation of protein profile in vitreous samples of patients with naive age-related macular degeneration using proteomic approaches. BMC Geriatr [Internet]. 2025 [cited 2026 Jan 27];25:1019. https://doi.org/10.1186/S12877-025-06655-5

62. Lopez ML, Kearns VR, Patterson EA, Curran JM. Passive nanorheological tool to characterise hydrogels. 2025;17:15338. https://doi.org/10.1039/d5nr00875a

63. Urbańska MA, Thakur SS, Kolenderska SM. OCT-based dynamic mechanical analysis of vitreous humour. Opt Lasers Eng. Elsevier Ltd; 2024;172. https://doi.org/10.1016/j.optlaseng.2023.107881

64. Schulz A, Wahl S, Rickmann A, Ludwig J, Stanzel B V., Von Briesen H, et al. Age-related loss of human vitreal viscoelasticity. Transl Vis Sci Technol. Association for Research in Vision and Ophthalmology Inc.; 2019;8. https://doi.org/10.1167/tvst.8.3.56